Calculating the Forces Created by an Electrodynamic Wheel Using a 2-D Steady-State Finite-Element Method

Jonathan Bird and Thomas A. Lipo, *Life Fellow, IEEE*

University of Wisconsin-Madison, Madison, WI 53706 USA.

We present a two-dimensional complex steady-state finite-element method for calculating the lift and thrust or breaking forces created when a magnetic rotor is translationally moved and rotated over a conducting sheet. The method replaces the magnetic rotor with an equivalent current sheet by equating the current sheet's and magnet rotor's magnetic vector potentials. We validate the steady-state method by comparing the forces with transient finite-element models. The utility of this steady-state model is that it enables a study of the effects of parameter changes for such a machine to be undertaken rapidly.

***Index Terms*—Eddy currents, electromagnetic analysis, finite-element methods, Halbach rotor, maglev.**

I. Introduction

THE simultaneous rotational and translational motion of magnets above a conductive, nonmagnetic track such as illustrated in Fig. 1, induces eddy currents in the track that can simultaneously create lift, F_L, and thrust, F_T, forces [1]–[11]. When the circumferential velocity, $v_c = \omega r_0$, of this electrodynamic wheel is somewhat greater than the translational velocity, v_x, thrust forces are generated, while larger breaking forces result when the circumferential velocity is less than the translational velocity [8]–[11].

In the past, moving magnet inductive devices have been analyzed using thick and thin plate approximations [10]–[19] in which the thickness of the plate, d, is assumed to be either much less than or much greater than the magnetic diffusion depth, δ. The thin plate approximation, promulgated by Maxwell [20]–[22], has been more frequently used for moving magnet problems since the conductor thickness is generally less than the diffusion depth over the speed range of interest. The induced currents are then assumed to be contained within an infinitesimally small thickness. While the thin and thick plate approximations have successfully modeled the general relationship between forces at limited velocities, the current density plots obtained in this paper, using finite-element analysis (FEA), shows that neither such approximation is reasonable for this machine (see Fig. 18).

Numerous two-dimensional lumped parameter models of linear induction motors (LIMs), which have similar changing and traveling fields, have also been developed [23]–[26]. Such models are attractive because they enable steady-state and transient behavior to be studied with minimal computational cost and often use established rotary machine techniques. However, developing such a model for this electrodynamic wheel would be inaccurate as it has a very short length, a nonuniform air gap, the track is nonmagnetic, and the field within the track lacks 2-D symmetry.

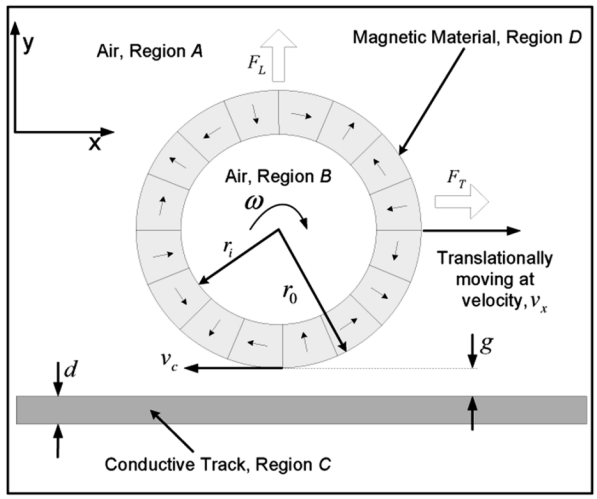

Fig. 1. A magnetic rotor translationally moving and rotating above a conductive, nonmagnetic track.

The solution of Maxwell's equations directly [14], [27], [28] or indirectly such as using Fourier transformation techniques [29]–[34] is also a common approach and can provide exact steady-state solutions. However, as there are rotating magnets with a nonuniform air gap this problem is not amenable to a closed form solution.

The exact modeling of such a device using numerical methods, such as FEA, is also problematic because of the need for a transient moving boundary. Although a number of commercial FEA packages can now model multiple moving boundaries [35], [36], the use of transient moving boundary simulations for parameter investigation is tediously time consuming. Furthermore, if the track region is transiently moved it cannot easily model high-speed translational motion since the moving track invariably reaches the end of the predefined movement region before attaining steady-state conditions; thus, leading to erroneous results.

Previously, Fujii used a 2-D transient technique to analyze the lift and thrust forces generated when radially positioned magnets are rotated over an aluminum track with back iron [36], [37]. In order to avoid modeling the rotating magnets, Fujii used a 2-D model with a poly-phase rotating current source in place of the transiently moving magnets. However, rather than using

Digital Object Identifier 10.1109/TMAG.2007.913038

Color versions of one or more of the figures in this paper are available online at http://ieeexplore.ieee.org.

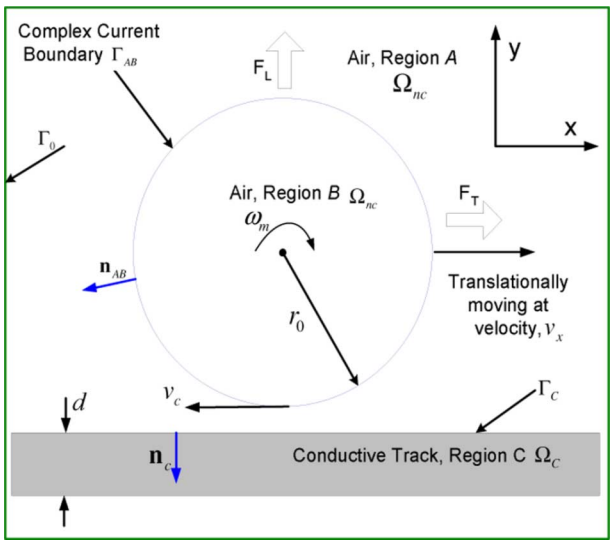

Fig. 2. Problem regions for an "equivalent" current sheet model.

a poly-phase current source, it is shown in this paper that an accurate model of the rotating magnets over a conductive track can be created using only a current sheet, such as shown in Fig. 2. When in addition the translational motion is modeled using the steady-state convective-diffusion equation within the track, then the magnets motion can be modeled using computationally efficient steady-state techniques. The accuracy of such a steady-state electrodynamic wheel model written in FEMLAB is confirmed by comparing the calculated force and power results with transient Magsoft Flux 2D FEA simulations.

The steady-state current sheet model neglects the permeability change within the magnet regions and the magnet eddy-current losses. However, since the magnet permeability is close to one, its neglect has minimal effect. Further, if the magnets are highly segmented, the eddy-current losses within the magnets are relatively minimal [38], [39].

II. Formulation

The applicable quasi-static Maxwell's equations are [28]

$$\nabla \times \mathbf{E} = -\frac{\partial \mathbf{B}}{\partial t} \tag{1}$$
$$\nabla \times \mathbf{H} = \mathbf{J} \tag{2}$$
$$\nabla \cdot \mathbf{B} = 0 \tag{3}$$
$$\mathbf{J} = \sigma(\mathbf{E} + \mathbf{v} \times \mathbf{B}) + \mathbf{J}^s \tag{4}$$
$$\nabla \cdot \mathbf{J} = 0 \tag{5}$$

where

σ = conductivity of track;
$\mathbf{v}$ = velocity of the conductive material;
$\mathbf{J}^s$ = an external excitation source;

For ease of analysis, the conductive material is assumed to move translationally rather than the magnets. The conductive material is assumed to be isotropic and linear. Using the generalized constitutive relation

$$\mathbf{B} = \mu_0(\mathbf{H} + \mathbf{M}) \tag{6}$$

and expressing $\mathbf{E}$ and $\mathbf{B}$ in terms of the magnetic vector potential, $\mathbf{A}$, and the electric scalar potential, V

$$\mathbf{E} = -\frac{\partial \mathbf{A}}{\partial t} - \nabla V \tag{7}$$
$$\mathbf{B} = \nabla \times \mathbf{A} \tag{8}$$

enables (2) and (5) to be rewritten as

$$\sigma \frac{\partial \mathbf{A}}{\partial t} + \nabla \times \left(\frac{\nabla \times \mathbf{A}}{\mu_0} - \mathbf{M} \right) - \sigma \mathbf{v} \times (\nabla \times \mathbf{A}) + \sigma \nabla V = \mathbf{J}^s \tag{9}$$

$$\nabla \cdot \left(\mathbf{v} \times (\nabla \times \mathbf{A}) - \frac{\partial \mathbf{A}}{\partial t} - \nabla V \right) \sigma = 0. \tag{10}$$

Using the identity

$$\nabla \times (\nabla \times \mathbf{A}) = \nabla(\nabla \cdot \mathbf{A}) - \nabla^2 \mathbf{A} \tag{11}$$

and the Coulomb gauge $\nabla \cdot \mathbf{A} = 0$, (9) and (10) reduce to

$$-\frac{\nabla^2 \mathbf{A}}{\mu_0} + \sigma \left(\frac{\partial \mathbf{A}}{\partial t} + \nabla V - \mathbf{v} \times (\nabla \times \mathbf{A}) \right) = \nabla \times \mathbf{M} + \mathbf{J}^s \tag{12}$$

$$\nabla \cdot (\mathbf{v} \times (\nabla \times \mathbf{A}) - \nabla V)\sigma = 0. \tag{13}$$

Equations (12) and (13) are known as the convective $\mathbf{A}V$–$\mathbf{A}$ formulation [40]–[43]. The electric scalar potential in (12) cannot be removed by using the $\mathbf{A}^*$ method [44], [45] because if ∇V is removed then trying to impose $\mathbf{J} \cdot n = 0$ on the boundary when $\mathbf{v} \times \mathbf{B} \neq 0$ will give erroneous results [46]. However, Rodger showed that the electric scalar potential can be replaced if the velocity term in (12) is rewritten using the identity [28]

$$\mathbf{v} \times (\nabla \times \mathbf{A}) = \nabla(\mathbf{v} \cdot \mathbf{A}) - (\mathbf{v} \cdot \nabla)\mathbf{A} - (\mathbf{A} \cdot \nabla)\mathbf{v} - \mathbf{A} \times (\nabla \times \mathbf{v}). \tag{14}$$

The third and fourth terms in (14) involve gradients of velocity, and are nonzero only when the track is rotating [47]. As it is assumed that the track motion involves only translational velocity (14) reduces to

$$\mathbf{v} \times (\nabla \times \mathbf{A}) = \nabla(\mathbf{v} \cdot \mathbf{A}) - (\mathbf{v} \cdot \nabla)\mathbf{A}. \tag{15}$$

Substituting (15) into (12) and taking the divergence on both sides results in all terms being zero except

$$\nabla \cdot \nabla(\mathbf{v} \cdot \mathbf{A}) - \nabla \cdot \nabla V = 0. \tag{16}$$

Therefore, from (16) it can be concluded that [48]

$$V = \mathbf{v} \cdot \mathbf{A} \quad [\mathrm{V}]. \tag{17}$$

Substituting (17) back into (12) and using (15) yields a formulation in terms of $\mathbf{A}$ alone [40], [41], [48], [49]

$$\nabla^2\mathbf{A}-\mu_0\sigma\left(\frac{\partial\mathbf{A}}{\partial t}+(\mathbf{v}\cdot\nabla)\mathbf{A}\right)=-\mu_0\nabla\times\mathbf{M}-\mu_0\mathbf{J}^s. \quad (18)$$

For this simple 2-D model, the conductive track is assumed to be moving only in the x-direction. Using subscripts to denote scalar directions enables (18) to be expressed as

$$\nabla^2 A_z-\mu_0\sigma\left(\frac{\partial A_z}{\partial t}+v_x\frac{\partial A_z}{\partial x}\right)=-\mu_0\nabla\times\mathbf{M}-\mu_0 J_z^s. \quad (19)$$

Within the nonconducting regions, A and B, shown in Fig. 1, (19) reduces to

$$\frac{\partial^2 A_z}{\partial x^2}+\frac{\partial^2 A_z}{\partial y^2}=0. \quad (20)$$

In the conductive track region, C, (19) becomes

$$\frac{\partial^2 A_z}{\partial x^2}+\frac{\partial^2 A_z}{\partial y^2}-\mu_0\sigma\left(\frac{\partial A_z}{\partial t}+v_x\frac{\partial A_z}{\partial x}\right)=0. \quad (21)$$

If the conductivity within the magnets is assumed to be zero, then the magnet region, D, simplifies to

$$\frac{\partial^2 A_z}{\partial x^2}+\frac{\partial^2 A_z}{\partial y^2}=-\mu_0\nabla\times\mathbf{M}. \quad (22)$$

III. Equivalent Current Sheet Density

Rather than modeling the magnet's rotational motion in FEA using a transient time-stepping rotating boundary method, it is proposed that the magnetic vector potential field created by the magnets be instead created using an equivalent, one-dimensional complex current sheet function on the outer boundary of the wheel, r_0, as shown in Fig. 2. In this case, the governing equation in polar coordinates in regions A, B, and D will be

$$\frac{1}{r}\frac{\partial A_z^j}{\partial r}+\frac{\partial^2 A_z^j}{\partial r^2}+\frac{1}{r^2}\frac{\partial^2 A_z^j}{\partial\theta^2}=-\mu_0 J_z^j(\theta)\delta(r-r_o) \quad (23)$$

where

A_z^j = vector potential due to the current sheet;
$J_z^j(\theta)$ = current sheet function (to be determined);
$\delta(r-r_o)$ = Dirac delta function [50].

Considering (22), it can be seen that the value of the magnetic vector potential, on the rotor edge, is due to the magnetization vector, $\mathbf{M}$. Therefore, if the magnitude of the magnetic potential, on the rotor edge, caused by the fictitious current sheet, is made to equal the magnitude of the magnetic potential on the rotor surface, r_0, due to the magnet's magnetization vector, i.e.,

$$A_z^j(r_0,\theta)=A_z^m(r_0,\theta) \quad (24)$$

where

A_z^j = magnetic potential on current sheet surface;
A_z^m = magnetic potential on magnetic rotor surface.

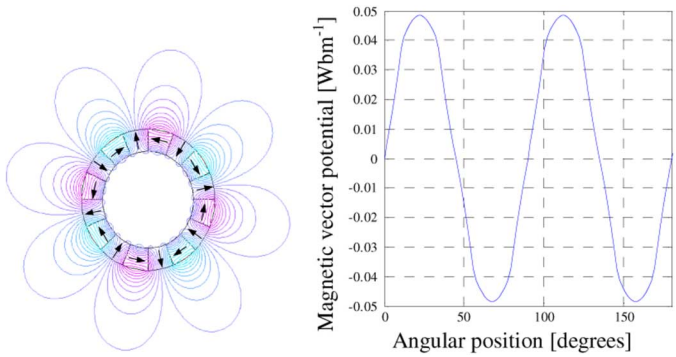

Fig. 3. Magnetic vector potential field plot for a four pole-pair Halbach rotor. The value on the rotor surface is also shown ($r_o = 0.25$ m, $r_i = 0.1865$ m, $B_r = 1.422$, $\mu_r = 1.055$).

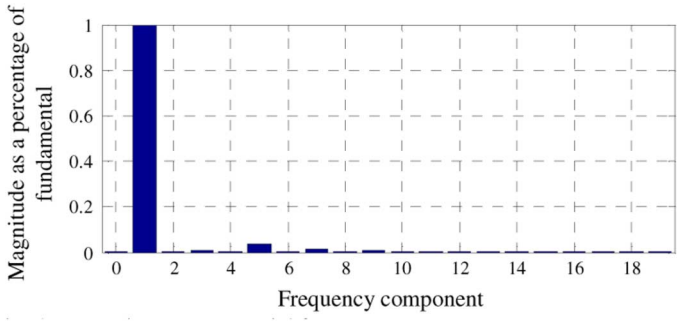

Fig. 4. Magnetic vector potential frequency components.

then the current sheet's vector potential on the rotor surface is forced to be equivalent. As shown, this results in equivalent forces being created.

To illustrate this method, a Halbach rotor with four pole-pairs is used [51]. The Halbach array creates an almost purely sinusoidal magnetic potential. For example, the field created by the four pole-pair Halbach rotor shown in Fig. 3 creates the magnetic potential on the rotor surface as shown to the right of Fig. 3. The corresponding harmonic component analysis, Fig. 4, confirms the field's almost sinusoidal form.

By using FEA, or analytically, the electrodynamic wheel's magnetic vector potential can be determined as a Fourier series. For the Halbach rotor, the field on the magnet surface can be modeled accurately using only the fundamental

$$A_z^m(r_o,\theta)=A_z^{m,\text{peak}}\sin(P\theta) \quad (25)$$

where

P = number of pole-pairs;
$A_z^{m,\text{peak}}$ = peak vector potential on the rotor surface.

In order to model the mechanical rotation in steady-state, a complex function must be used

$$J_z^j(\theta)=J_z^{\text{Peak}}e^{jP\theta}. \quad (26)$$

Thus, (23) becomes

$$\frac{1}{r}\frac{\partial A_z^j}{\partial r}+\frac{\partial^2 A_z^j}{\partial r^2}+\frac{1}{r^2}\frac{\partial^2 A_z^j}{\partial\theta^2}=-\mu_0 J_z^{\text{peak}}e^{jP\theta}\delta(r-r_o). \quad (27)$$

Equation (27) must be solved in order to determine the value of the equivalent current on the rotor surface. By observation, the potential solution will have the form

$$A_z^j(r,\theta) = a(r) J_z^{\text{Peak}} e^{jP\theta}. \tag{28}$$

Substituting (28) into (27) allows the angular dependence in (27) to be cancelled out, leading to

$$\frac{\partial^2 a}{\partial r^2} + \frac{1}{r}\frac{\partial a}{\partial r} - \frac{P^2 a}{r^2} = -\mu_0 \delta(r - r_o). \tag{29}$$

The complementary solution to (29) is obtained by solving

$$r^2 \frac{\partial^2 a_c}{\partial r^2} + r\frac{\partial a_c}{\partial r} - P^2 a_c = 0 \tag{30}$$

which is the Cauchy–Euler equation [52]. It has the solution in the form

$$a_c(r) = r^m \tag{31}$$

where m must be determined. Substituting (31) into (30) gives

$$(m^2 - P^2) r^m = 0. \tag{32}$$

Thus, $m = \pm P$, and hence, the general solution to (30) is

$$a_c(r) = c_1 r^P + c_2 r^{-P}. \tag{33}$$

Knowing the complementary solution enables the complete solution to (29) to be obtained by using the variation of parameters method [52] whereby the coefficients c_1 and c_2 are replaced with variables $u_1(r)$ and $u_2(r)$ such that

$$a(r) = u_1(r) r^P + u_2(r) r^{-P} \tag{34}$$

is a solution to (29). The evaluation of the variables is determined by integrating [52]

$$\frac{du_1}{dr} = -\frac{a_2 f(r)}{W} \tag{35}$$

$$\frac{du_2}{dr} = \frac{a_1 f(r)}{W} \tag{36}$$

where

$$f(r) = -\mu_0 \delta(r - r_o) \tag{37}$$

$$a_1 = r^P \tag{38}$$

$$a_2 = r^{-P} \tag{39}$$

$$W = \begin{vmatrix} a_1 & a_2 \\ \frac{\partial a_1}{\partial r} & \frac{\partial a_2}{\partial r} \end{vmatrix} = \begin{vmatrix} r^P & r^{-P} \\ Pr^{P-1} & -Pr^{-P-1} \end{vmatrix} = \frac{-2P}{r} \tag{40}$$

W is the Wronskian [52]. Evaluating (35) and (36) yields

$$u_1 = -\frac{\mu_0}{2P}\int_0^\infty r^{-P} r \delta(r - r_o) dr = -\mu_0 \frac{r_o^{-P+1}}{2P} \tag{41}$$

$$u_2 = \frac{\mu_0}{2P}\int_0^\infty r^{P} r \delta(r - r_o) dr = \mu_0 \frac{r_o^{P+1}}{2P}. \tag{42}$$

The presence of the delta function results in u_1 and u_2 being constants. Substituting (41) and (42) into (34) gives

$$a(r) = \frac{\mu_0 r_o}{2P}\left(\frac{r_o^P}{r^P} - \frac{r^P}{r_o^P}\right). \tag{43}$$

When $r > r_o$, the magnitude of (43) must decrease with increasing radii, therefore, outside the rotor

$$a(r) = \frac{\mu_0 r_o}{2P}\left(\frac{r_o^P}{r^P}\right). \tag{44}$$

Substituting (44) into (28) gives the complete solution for the vector potential field outside the rotor as

$$A_z^j(r,\theta) = \frac{\mu_0 J_z^{\text{Peak}} r_o}{2P}\left(\frac{r_o^P}{r^P}\right) e^{jP\theta}. \tag{45}$$

Therefore, once the peak magnetic vector potential on the rotor surface is determined, the equivalent peak sinusoidal current sheet value on the rotor surface will be

$$J_z^{\text{Peak}} = \frac{2P}{\mu_0 r_o} A_z^{m,\text{Peak}}. \tag{46}$$

IV. The Complex Steady-State Model

The steady-state magnetic potential solution has the form

$$A_z(x,y,t) = A_z(x,y) e^{j\omega t}. \tag{47}$$

Therefore, the steady-state form of (21) is then

$$\frac{\partial^2 A_z}{\partial x^2} + \frac{\partial^2 A_z}{\partial y^2} - \mu_0 \sigma\left(j\omega A_z + v_x \frac{\partial A_z}{\partial x}\right) = 0 \tag{48}$$

and the problem boundary conditions are

$$\mathbf{n}_{AB} \times (\mathbf{B}^A - \mathbf{B}^B) = \frac{2P A_z^{m,\text{Peak}}}{\mu_0 r_o} e^{jP\theta} \text{ on } \Gamma_{AB} \tag{49}$$

$$\mathbf{n}_c \times (\mathbf{B}^C - \mathbf{B}^A) = 0 \text{ on } \Gamma_c \tag{50}$$

$$\mathbf{n}_c \cdot (\mathbf{B}^C - \mathbf{B}^A) = 0 \text{ on } \Gamma_c \tag{51}$$

$$A_z = 0 \text{ on } \Gamma_0. \tag{52}$$

The complex steady-state model was validated by using a number of transient FEA simulations. The validation was made difficult because the available commercial FEA versions could not simultaneously model translational and rotational motion or fictitious current sheets. Therefore, three transient models were created in order to validate the steady-state current sheet model. First, the current sheet model was compared with a transiently rotating Halbach magnet array rotor over a conductive track, with no translation. Second, a three-phase steady-state current source model, as used by Fujii [36], [37], was validated. Third, a combined transient three-phase current source model with a transient moving track model was created. The three transient models and their comparisons with the steady-state model are

TABLE I
SIMULATION PARAMETERS

Translational Velocity, v_t	0 ms^{-1}
Angular Velocity, v_r	Varied
Outer radius, r_0	0.3 m
Inner radius, r_i	0.1725 m
Track Thickness, t	15 mm
Track Conductivity, σ	3.5×10^7 Sm^{-1}
Air gap, g	10 mm
Pole pairs, P	4
Magnet Width, w	0.3 m
Magnet Residual Flux Density, B_r	1.42 T
Magnet Permeability, μ_r	1.08
Peak Vector Potential on Rotor Surface, $A_{z,peak}^m$	0.069 Wbm^{-1}
Peak Current Sheet Density, J_z^{peak}	1.46×10^6 Am^{-1}

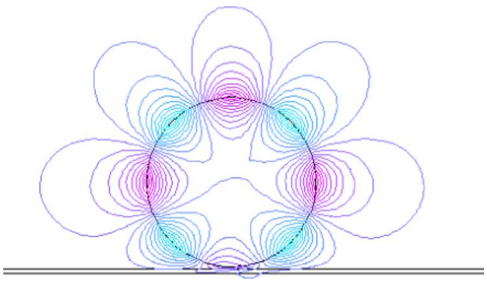

Fig. 5. Steady-state vector potential contour plot for a current sheet rotor at 1000 RPM.

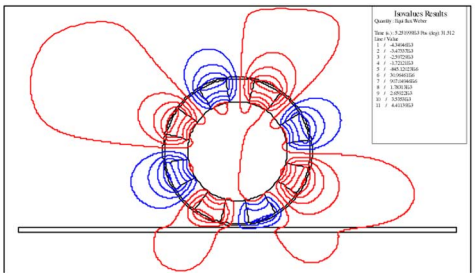

Fig. 6. Magsoft Flux 2D Halbach rotor magnetic field transient simulation contour plot at one time step value.

presented below. The force in the track was computed using Lorentz's force

$$F_T = w \int \mathrm{Re}(J_z)\mathrm{Re}(B_y)dS \tag{53}$$

$$F_L = w \int \mathrm{Re}(J_z)\mathrm{Re}(B_x)dS \tag{54}$$

where w is the magnet and track width.

A. A Steady-State Current Sheet Model and a Transient Halbach Rotor Model

Using the parameters given in Table I, the steady-state current sheet model created in FEMLAB v3.1, and shown in Fig. 5, was compared with a Magsoft Flux 2D transient Halbach rotor model, Fig. 6. The flux compression is clearly visible between the track and the wheel. A comparison of the thrust, lift, and power loss between the steady-state and transient FEA models is shown in Figs. 7 and 8. The Magsoft transient force and power results for the 0.3 m Halbach rotor at 1000 RPM is shown in

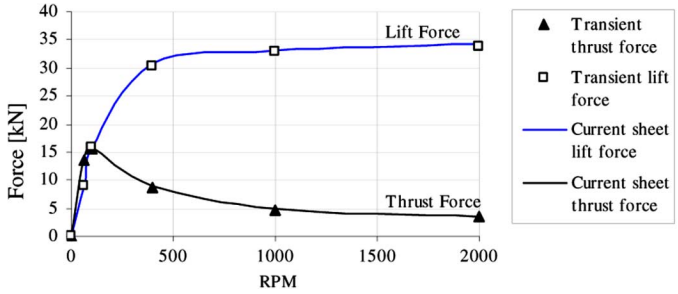

Fig. 7. Thrust and lift force comparison for the steady-state current sheet model and the Magsoft Flux 2D transient Halbach model with four pole-pairs.

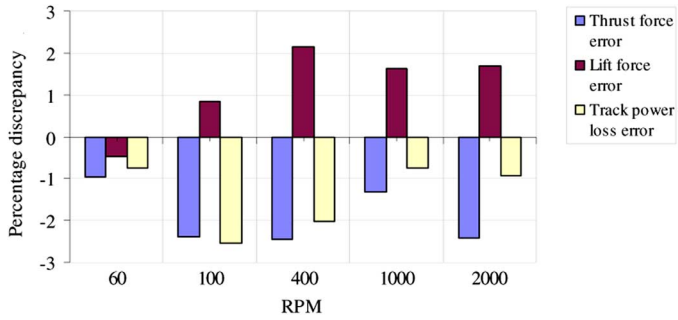

Fig. 8. Error comparison between the steady-state current sheet model and the transient FEA model with four pole-pair rotor.

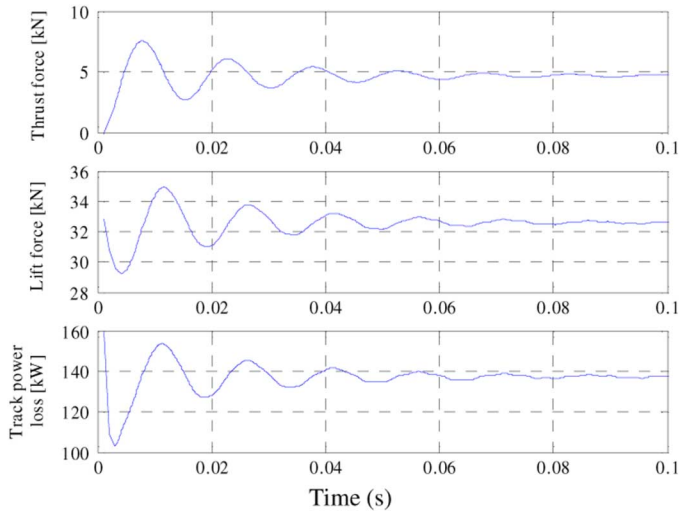

Fig. 9. Magsoft Flux 2D transient results at 1000 RPM for the four pole-pair Halbach rotor.

Fig. 9. Similar accuracy was obtained for three and five pole-pair models.

B. A Steady-State Current Source Model and a Transient Halbach Model—No Translational Motion

Due to the need to transiently model both the rotating magnets and a moving track using Magsoft Flux 2D, the rotational motion of the magnet was modeled using an equivalent three-phase current, as shown in Fig. 10. The value of the current density, that created the equivalent rotor surface magnetic vector potential, was determined to be 3.17×10^7 Am^{-2}. It was chosen by

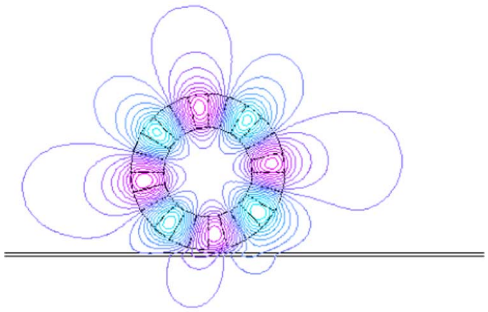

Fig. 10. Three-phase current source model of a four pole-pair Halbach rotor.

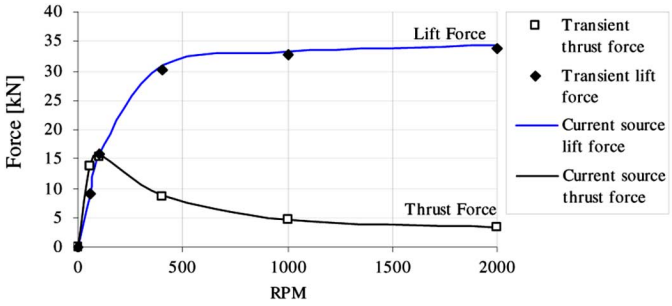

Fig. 11. Thrust and lift force comparison for the three-phase current source model and the Magsoft Flux 2D transient Halbach model with four pole-pair rotor.

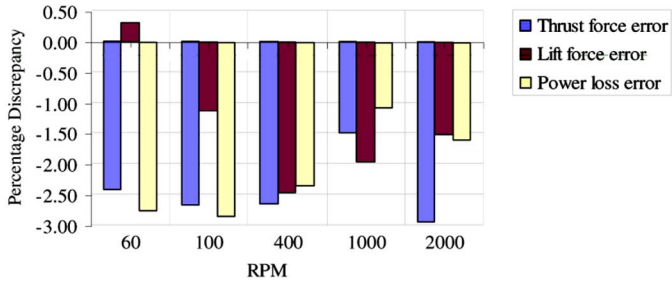

Fig. 12. Numerical error between the three-phase current source model and transient Magsoft model for a four pole-pair rotor.

comparing the current source with Halbach rotor's vector potential, A_z^m. The validity of the three-phase model was confirmed by comparing it with the transient model. The force and power loss comparison is shown in Figs. 11 and 12.

C. Steady-State Current Sheet Model and a Magsoft Transient Moving Track With a Three-Phase Current Source

Lastly, the current-sheet steady-state model with translational motion was verified by comparing it with the Magsoft Flux 2D transient model that had both a translationally moving conducting track and a three-phase rotating current source. The field lines for the Magsoft model is shown in Fig. 13. The transient translational motion in Magsoft is accounted for by defining a moveable track region, therefore in order to ensure steady-state values are reached only low translational speeds are used. The transient results for 1 ms^{-1} translational speed and 150 RPM ($\nu_c = 4.7\ \text{ms}^{-1}$) is shown in Fig. 14. Interestingly, the transient results almost reach a non-oscillatory steady-state. The comparison between the two models is shown in Figs. 15 and 16. The

Fig. 13. Magsoft Flux 2D transient model with a rotating three-phase current source and a translationally moving track at one time step.

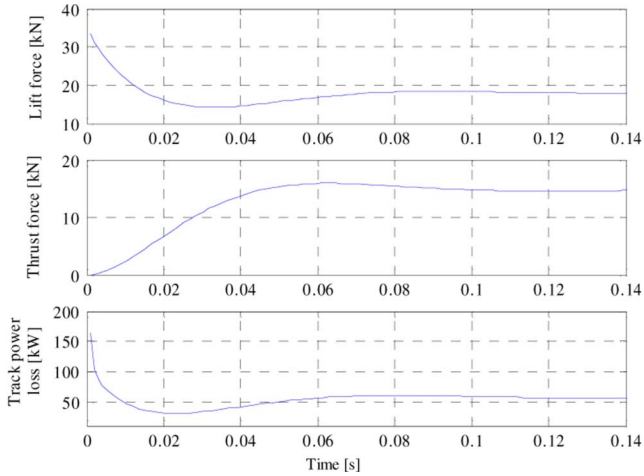

Fig. 14. Magsoft transient results for 1 ms^{-1} translational velocity and 150 RPM.

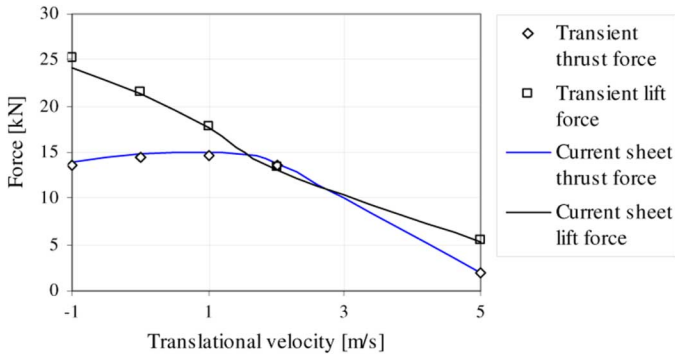

Fig. 15. A thrust and lift forces comparison between the steady-state current sheet model and transient Magsoft Flux 2D model at 150 RPM.

comparison confirms the accuracy of this steady-state current sheet method.

V. Discussion

The use of rotating magnets to induce the track currents rather than using a linear induction motor circumvents the problems associated with operating at a low power factor. To observe just how inductive the operation of the electrodynamic wheel is, the power factor can be computed from the complex power, S, on

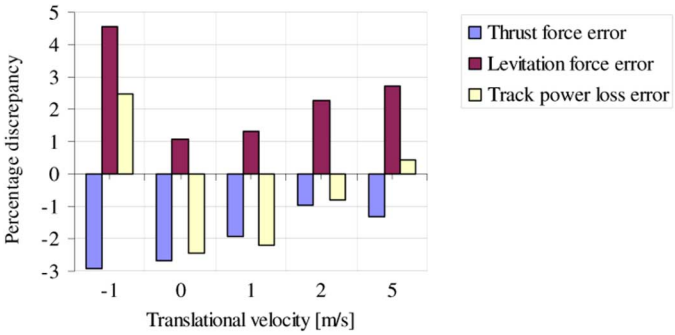

Fig. 16. Error between the steady-state current sheet model and the transient three-phase Magsoft model.

TABLE II
PARAMETERS USED TO COMPUTE THE COMPLEX POWER

Translational velocity, v_t	89.4 ms^{-1} (200miles/hour)
Slip, s	Varied
Outer radius, r_o	0.24 m
Inner radius, r_i	0.13 m
Pole pairs, P	3
Track conductivity, σ	3.5×10^7 Sm^{-1}
Track thickness, d	10 mm
Model width, w	0.4 m
Air gap, g	10 mm
Current sheet density	1.3394×10^6 Am^{-1}

the fictitious current sheet boundary

$$S = \frac{w}{2}\int_0^{2\pi} J_z^{j*}(\theta)E_z d\theta = P + jQ \quad [\text{VA}] \qquad (55)$$

where

w = width of track and magnet model;
P = real power loss;
Q = reactive power.

The input power can also be computed from

$$P = T\omega \quad [\text{W}] \qquad (56)$$
$$= F_T v_t + P_{\text{Loss}} \quad [\text{W}]. \qquad (57)$$

As an example, using the parameters shown in Table II the thrust and lift force relationship, as a function of slip, calculated using the current sheet model for a 200 mi/h translational velocity is shown in Fig. 17. Using (55) the complex power at 20 ms^{-1} slip is $S = 2.22 \times 10^5 + 334 \times 10^7 \text{j}$ VA. This result corresponds to a power factor, $\text{pf} = 0.007$. Clearly, this is an untenable operating regime if the rotating field was created by three-phase currents rather than rotating magnets.

The current density distribution within the conducting track at the slip value of 20 ms^{-1} is illustrated in Fig. 18. Its nonuniform distribution shows that it would have been unreasonable to assume that the current is uniformly distributed throughout the track thickness.

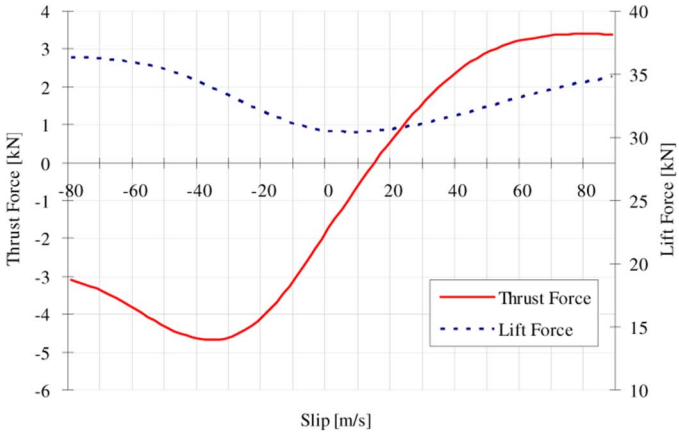

Fig. 17. Example of the lift and thrust force relationship for a 200 mi/h (89.4 ms^{-1}) translational velocity.

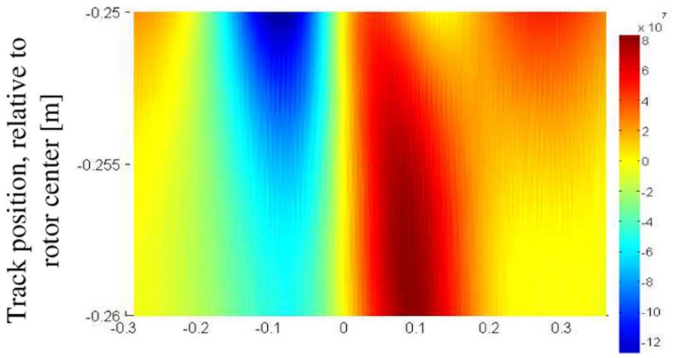

Fig. 18. Current density [Am^{-2}] within track for the steady-state simulation with a 89.4 ms^{-1} translational velocity and a 20 ms^{-1} slip.

VI. CONCLUSION

The modeling of the high-speed rotational and translational motion of magnets above a conductive, nonmagnetic track is typically highly time consuming and computationally expensive if transient models are used. However, modeling the rotating magnets with a complex current sheet and using the convective-diffusion equation to account for the translational motion enables a fast steady-state model to be used. The accuracy of such a steady-state model was confirmed by comparing it with transient finite-element simulations. A steady-state model enables a parameter investigation and performance assessment of an electrodynamic wheel to be quickly undertaken. A 2-D parameter and performance investigation of the electrodynamic wheel is presented in a companion paper [53].

ACKNOWLEDGMENT

The authors would like to acknowledge the support provided by the member companies of the Wisconsin Electric Machines and Power Electronics Consortium (WEMPEC) at the University of Wisconsin-Madison. Also, the authors would gratefully like to thank the Magsoft Corporation for the use of their FEA software.

REFERENCES

[1] M. Kawai and H. Ariga, "Equos-LIM-CAR," (in Japanese) *The Invention*, vol. 89, pp. 70–77, 1992.

[2] N. Fujii *et al.*, "Three dimensional force of magnet wheel with revolving permanent magnets," *IEEE Trans. Magn.*, vol. 33, no. 5, pp. 4221–4223, Sep. 1997.
[3] N. Fujii *et al.*, "Characteristics of magnetic lift, propulsion and guidance by using magnet wheels with rotating permanent magnets," in *IEEE Ind. Appl. Conf.*, 2000, pp. 257–262.
[4] N. Fujii *et al.*, "Basic characteristics of magnet wheels with rotating permanent magnets," in *IEEE Ind. Appl. Conf.*, 1994, pp. 203–209.
[5] N. Fujii *et al.*, "Revolving magnet wheels with permanent magnets," *Electr. Eng. Jpn.*, vol. 116, pp. 106–117, 1996.
[6] I. Boldea and S. A. Nasar, *Linear Motion Electromagnetic Systems*. New York: Wiley, 1985, pp. 461–478.
[7] Philco-Ford, "Department of Transportation, Conceptual Design and Analysis of the Tracked Magnetically Levitated Vehicle Technology Program (TMLV)—Repulse Scheme Volume 1—Technical Studies," Department of Transport, Springfield, VA, Tech. Rep. DOT-FR-40024 (Task I), Feb. 1975.
[8] J. Bird and T. A. Lipo, "An electrodynamic wheel: An integrated propulsion and levitation machine," in *Elect. Mach. Drives Conf.*, 2003, pp. 1410–1416.
[9] J. Bird, "An investigation into the use of electrodynamic wheels for high-speed ground transportation," Ph.D. thesis, Dept. Electr. Eng., Univ. Wisconsin-Madison, Madison, WI, 2007.
[10] R. H. Borcherts and L. C. Davis, "The superconducting paddle-wheel as an integrated propulsion levitation machine for high speed ground transportation," *Electr. Mach. Electrom.*, vol. 3, pp. 341–355, Apr.–Jun. 1979.
[11] L. C. Davis and R. H. Borcherts, "Superconducting paddle wheels, screws, and other propulsion units for high-speed ground transportation," *J. Appl. Phys.*, vol. 44, pp. 3294–3299, Jul. 1973.
[12] L. T. Klauder, "A magnetic field diffusion problem," *Amer. J. Phys.*, vol. 37, pp. 323–325, Mar. 1969.
[13] P. L. Richards and M. Tinkham, "Magnetic suspension and propulsion systems for high-speed transportation," *J. Appl. Phys.*, vol. 43, pp. 2680–2691, Jun. 1972.
[14] R. L. Byer *et al.*, "Superconducting, magnetically levitated merry-go-round," *Amer. J. Phys.*, vol. 42, pp. 111–125, 1974.
[15] S. W. Lee and R. Menendez, "Forces at low-and high-speed limits in magnetic levitation systems," *J. Appl. Phys.*, vol. 46, pp. 422–425, 1975.
[16] L. C. Davis, "Drag force on a magnet moving near a thin conductor," *J. Appl. Phys.*, vol. 43, pp. 4256–4257, 1972.
[17] L. C. Davis and J. Reitz, "Eddy currents in finite conducting sheets," *J. Appl. Phys.*, vol. 42, pp. 4119–4127, Oct. 1971.
[18] D. Schieber, "Principles of operation of linear induction devices," *Proc. IEEE*, vol. 61, no. 5, pp. 647–656, May 1973.
[19] B. T. Ooi and D. C. White, "Traction and normal forces in the linear induction motor," *IEEE Trans. Power App. Syst.*, vol. PAS-89, no. 4, pp. 638–645, Apr. 1970.
[20] J. Maxwell, "On the induction of electric currents in an infinite plane sheet of uniform conductivity," *Proc. Roy. Soc. London*, vol. A20, 1872.
[21] J. Maxwell, *A Treatise on Electricity & Magnetism*. New York: Dover, 1954, vol. 2, pp. 286–314.
[22] W. M. Saslow, "Maxwell's theory of eddy currents in thin conducting sheets and applications to electromagnetic shielding and MAGLEV," *Amer. J. Phys.*, vol. 60, pp. 693–711, Aug. 1992.
[23] B. T. Ooi, "A generalized machine theory of the linear induction motor," *IEEE Trans. Power App. Syst.*, vol. PAS-92, no. 4, pp. 1252–1259, Jul./Aug. 1973.
[24] T. A. Lipo and T. A. Nodahl, "Pole-by-pole d-q model of a linear induction machine," *IEEE Trans. Power App. Syst.*, vol. PAS-98, no. 2, pp. 629–639, Mar./Apr. 1979.
[25] R. M. Pai *et al.*, "A complete equivalent circuit of a linear induction motor with sheet secondary," *IEEE Trans. Magn.*, vol. 24, no. 1, pp. 639–653, Jan. 1988.
[26] J. Faiz and H. Jafari, "Accurate modeling of single-sided linear induction motor considers end effect and equivalent thickness," *IEEE Trans. Magn.*, vol. 36, no. 5, pp. 3785–3790, Sep. 2000.
[27] R. J. Hill, "Teaching electrodynamic levitation theory," *IEEE Trans. Educ.*, vol. 33, no. 4, pp. 346–354, Nov. 1990.
[28] J. D. Jackson, *Classical Electrodynamics*, 3rd ed. New York: Wiley, 1999, pp. 218–223.
[29] S. Lee and R. C. Menendez, "Force on current coils moving over a conducting sheet with application to magnetic levitation," *Proc. IEEE*, vol. 62, no. 5, pp. 567–577, May 1974.
[30] J. R. Reitz and L. C. Davis, "Force on a rectangular coil moving above a conducting slab," *J. Appl. Phys.*, vol. 43, pp. 1547–1553, Apr. 1972.
[31] R. H. Borcherts and L. C. Davis, "Force on a coil moving over a conducting surface including edge and channel effects," *J. Appl. Phys.*, vol. 43, pp. 2418–2427, May 1972.
[32] E. M. Freeman and C. Papageorgiou, "Spatial Fourier transforms: A new view of end effects in linear induction motors," *Proc. Inst. Elect. Eng.*, vol. 125, pp. 747–753, Aug. 1978.
[33] S. Yamamura, *Theory of Linear Induction Motors*. Tokyo, Japan: Univ. Tokyo Press, 1979, pp. 3–123.
[34] K. Oberretl, , E. R. Laithwaite, Ed., "Three-dimensional analysis of the linear motor," in *Transport Without Wheels*. London, U.K.: Elek Books Ltd., 1977, pp. 217–248.
[35] Version 6.15 of MagNet. Infolytica Corporation, 2004.
[36] N. Fujii *et al.*, "Characteristics of a moving magnet rotator over a conducting plate," *IEEE Trans. Magn.*, vol. 41, no. 10, pp. 3811–3813, Oct. 2005.
[37] N. Fujii *et al.*, "Simple end effect compensator for linear induction motor," *IEEE Trans. Magn.*, vol. 38, no. 5, pp. 3270–3272, Sep. 2002.
[38] K. Atallah *et al.*, "Rotor loss in permanent-magnet brushless AC machines," *IEEE Trans. Ind. Appl.*, vol. 36, no. 6, pp. 1612–1618, Nov./Dec. 2000.
[39] H. Toda *et al.*, "Rotor eddy-current loss in permanent magnet brushless machines," *IEEE Trans. Magn.*, vol. 40, no. 4, pp. 2104–2106, Jul. 2004.
[40] D. Rodger and H. C. Lai, "A comparison of formulations for 3D finite element modeling of electromagnetic launchers," *IEEE Trans. Magn.*, vol. 37, no. 1, pp. 135–138, Jan. 2001.
[41] Y. Marechal *et al.*, "Computation of 3D eddy currents in moving conductors of electromagnetic retarders," in *Int. Conf. Computation in Electromagnetics*, London, U.K., Nov. 1991, pp. 25–27.
[42] H. Song and N. Ida, "Modeling of velocity terms in 3D eddy current problems," *IEEE Trans. Magn.*, vol. 28, no. 2, pp. 1178–1181, Mar. 1992.
[43] K. Muramatsu *et al.*, "Method for analyzing eddy currents in moving conductors," *Electr. Eng. Jpn.*, vol. 114, pp. 102–113, Jul. 1994.
[44] C. R. I. Emson and J. Simkin, "An optimal method for 3-D eddy currents," *IEEE Trans. Magn.*, vol. MAG-19, no. 6, pp. 2450–2452, Nov. 1983.
[45] D. Rodger and J. Eastham, "A formulation for low frequency eddy current solutions," *IEEE Trans. Magn.*, vol. MAG-19, no. 6, pp. 2450–2452, Nov. 1983.
[46] D. Rodger *et al.*, "A formulation for 3D moving conductor eddy current problems," *IEEE Trans. Magn.*, vol. 25, no. 5, pp. 4147–4149, Sep. 1989.
[47] N. Allen *et al.*, "Towards increased speed computations in 3D moving eddy current finite element modelling," *IEEE Trans. Magn.*, vol. 31, no. 6, pp. 3524–3526, Nov. 1995.
[48] D. Rodger *et al.*, "An optimal formulation for 3D moving conductor eddy current problems with smooth rotors," *IEEE Trans. Magn.*, vol. 26, no. 5, pp. 2359–2363, Sep. 1990.
[49] S. Williamson and E. K. C. Chan, "Three-dimensional finite-element formulation for problems involving time-varying fields, relative motion, and magnetic saturation," *Inst. Elect. Eng. Proc. A*, vol. 140, pp. 121–130, Mar. 1993.
[50] J. Nilsson and S. A. Riedel, *Electric Circuits*, 5th ed. Reading, MA: Addison-Wesley, 1996, pp. 552–556.
[51] K. Halbach, "Design of permanent multipole magnets with oriented rare earth cobalt material," *Nucl. Instrum. Methods*, vol. 187, pp. 1–10, 1980.
[52] D. G. Zill, *A First Course in Differential Equations With Applications*, 3rd ed. Boston, MA: PWS, 1986, pp. 172–181.
[53] J. Bird and T. A. Lipo, "Characteristics of an electrodynamic wheel using a 2-D steady-state model," *IEEE Trans. Magn.*, vol. 43, no. 8, pp. 3395–3405, Aug. 2007.

Manuscript received July 13, 2006; revised November 14, 2007. Corresponding author: J. Bird (e-mail: jonathan.bird@ieee.org).